A New Test Procedure to Measure Power Electronic Devices' Frequency Coupling Admittance

Daniele Gallo, *Member, IEEE*, Roberto Langella, *Senior Member, IEEE*, Mario Luiso, *Member, IEEE*, Alfredo Testa, *Fellow, IEEE*, and Neville R. Watson, *Senior Member, IEEE*

***Abstract*— One method to model power electronic devices for harmonic emission studies is using frequency-domain models based on the frequency coupling matrices. This paper presents a new test procedure for the experimental evaluation of the frequency coupling matrix elements of power electronic devices. An automated test system is designed, realized, and characterized from a metrological perspective. Experimental tests show the tremendous increase in speed of the new test procedure in comparison to the classical test procedures present in the literature, with the same levels of accuracy of obtained results.**

***Index Terms*— Admittance, frequency coupling matrix, harmonics, phase-dependent characteristics, power electronics, power quality, power system measurement.**

I. Introduction

THERE is an increasing need to model the harmonic emission of modern power electronic devices in distribution networks. This need is a result of more and more household appliances, as well as industrial loads, utilizing power electronic interfaces [i.e., heat and ventilation air conditioning systems, electric vehicles, compact florescent lamp (CFLs), LEDs, variable speed drives, and so on]. In order to predict the cumulative impact in terms of voltage harmonic distortion, fast and accurate models are necessary [1].

Different methods for harmonic analysis in the frequency domain and time domain are currently present in the relevant literature; hybrid frequency and time-domain methods have also been developed [2]–[14]. Medina *et al*. [2] present a review with a concise description and analysis of the fundamentals, characteristics, analytical details, merits, and drawbacks associated with existing methods in frequency and time domains for harmonic analysis in practical power networks. Concerning frequency domain methods [2] introduce six categories: 1) direct method; 2) iterative harmonic analysis; 3) harmonic power flow method; 4) dynamic harmonic domain method; 5) frequency coupled matrix method; and 6) multiphase harmonic analysis.

Frequency coupled (or transfer) matrix methods are able to model the sensitivity of the current harmonic emission of the majority of power electronic devices to the phase angle of the background (BG) voltage harmonics. This sensitivity can be modeled by Norton equivalent models based on cross-coupling admittance matrices using linearization of the power electronic devices around a suitable base working point. The necessity of a phase-dependent relationship between the transfers of voltage and current was demonstrated for the first time in [3]. In [4], a linearized cross-coupled admittance was obtained for a high voltage direct current converter; the admittance lattice structure was sparse, and included the phase dependence by tensor representation.

Frequency transfer matrices (FTMs) can be obtained analytically [4]–[6] (very difficult and device sensitive) or by means of time-domain simulations or experimental tests [7]–[12] (very practical and, in principle, applicable to all loads). In [7], a sequential harmonic injection technique was introduced to experimentally obtain the FTM by applying small input (voltage) distortions to the load and measuring the change in the output (current). The phase and magnitude of the distortion were varied to investigate the phase-dependent relationships and to confirm the device's linearity around the operating point.

The accuracy of such approaches mainly depends on two aspects: 1) the fulfillment of the linearization hypothesis around a stable base point (linearity hypothesis) and 2) the accuracy of the experimental test procedure used to evaluate the FTM (generation and measurement uncertainty), which has been under evaluated in the literature.

In [15], the second aspect was investigated with the aim of highlighting the main accuracy issues that have to be considered during such kind of experimental activities. This paper builds on the initial work presented in [15], which is here significantly extended here by providing: 1) a new test procedure; 2) a full metrological characterization of the experimental setup; and 3) a more comprehensive set of experimental results.

It is shown that compared to the classical test procedures present in the literature, the new test procedure provides a significant reduction in experimental time without reducing the accuracy of the obtained results.

Manuscript received November 13, 2017; revised February 2, 2018; accepted March 4, 2018. Date of publication April 25, 2018; date of current version September 17, 2018. This work was supported by the Italian Ministry of University and Research under Grant PON03PE-00175-1, Grant PON03PE-00177-1, and Grant PON03PE-00178-1. The Associate Editor coordinating the review process was Dr. Roberto Ferrero. *(Corresponding author: Roberto Langella.)*

D. Gallo, R. Langella, M. Luiso, and A. Testa are with the Department of Engineering, University of Campania "Luigi Vanvitelli," 81100 Aversa, Italy (e-mail: daniele.gallo@unicampania.it; roberto.langella@unicampania.it; mario.luiso@unicampania.it; alfredo.testa@unicampania.it).

N. R. Watson is with the Department of Electrical and Computer Engineering, University of Canterbury, Christchurch 8041, New Zealand (e-mail: neville.watson@canterbury.ac.nz).

Color versions of one or more of the figures in this paper are available online at http://ieeexplore.ieee.org.

Digital Object Identifier 10.1109/TIM.2018.2819318

II. Frequency Transfer Matrix

A. Review of FTM Approach

Under small-signal operation, a device can be linearized around an operating point. This linear gradient can be represented by a Norton admittance term that can be considered either constant or, if more accuracy is required, variable with the operating conditions.

A generic hth terminal harmonic current, I_h, is calculated by the following equation and is the sum of the base case current, I_{bh}, and the current deviation, ΔI_h, caused by the voltage distortion, $\Delta V = [\Delta V_1, \Delta V_2, \ldots, \Delta V_K,]^T$, across the FTM Y, whose terms $Y_{h|k}$, relate the kth harmonic voltage to the hth harmonic current

$$\begin{bmatrix} I_1 \\ I_2 \\ \vdots \\ I_H \end{bmatrix} = \begin{bmatrix} Y_{1|1} & Y_{1|2} & \ldots & Y_{1|K} \\ Y_{2|1} & Y_{2|2} & \ldots & Y_{2|K} \\ \vdots & \vdots & \ddots & \vdots \\ Y_{H|1} & Y_{H|2} & \ldots & Y_{H|K} \end{bmatrix} \begin{bmatrix} \Delta V_1 \\ \Delta V_2 \\ \vdots \\ \Delta V_K \end{bmatrix} + \begin{bmatrix} I_{b1} \\ I_{b2} \\ \vdots \\ I_{bH} \end{bmatrix}. \tag{1}$$

For developing the cross-coupling matrices, the positive and negative frequencies can be considered fully combined into the same matrix such that only positive harmonics need to be considered. The inclusion of positive and negative frequencies results in phase dependent transfers between the BG voltage harmonic and harmonic currents at all frequencies [4]. This phase dependent transfers can be elegantly modeled by introducing a tensor matrix, whose elements are real-valued matrices when rectangular coordinates are used instead of the complex-valued direct and negative frequency admittance matrices [5]. This improves the computational performance of the model. Tensors parameterization can be conducted in a very robust way using Fourier descriptors as proposed in [7] and discussed in [11] and [12].

B. Classical Measurement Method

Direct measurement of the elements of the FTM can be performed by sequentially applying a voltage distortion of a given magnitude and frequency and varying the phase angle from 0 to 2π in a discrete number of N_θ values. The following conditions have to be assumed: 1) the load is in steady-state condition and its frequency characteristics are time invariant; 2) the input is independent of the device operation (low supply impedance); and 3) the base case operating condition remains constant.

For each harmonic voltage magnitude and order k, the elements of (1), $Y_{h|k}$, with $h = 1, \ldots, H$, are calculated using

$$Y_{h|k}\ (\theta_i) = \frac{I_h(\theta_i) - I_{bh}}{\Delta V_k(\theta_i)} = \frac{\Delta I_{h|k}(\theta_i)}{\Delta V_k(\theta_i)} \quad \text{with } i = 1, \ldots, N_\theta. \tag{2}$$

Successively, tensor parameterization procedures, such as those presented in [7] and discussed in [11] and [12], can be applied to evaluate the elements of $\boldsymbol{Y}$. Taking more samples, i.e., higher values of N_θ, will not only increase the accuracy of the estimation but will also increase the duration of the experimental test activity to be conducted.

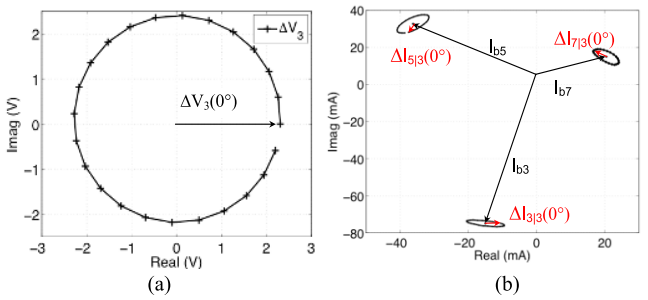

Fig. 1. CFL lamp. (a) Locus of ΔV_3 with varying phase angles in the range 0–2π; (b) loci of $I_{h|3}$ together with the corresponding base currents, I_{bh}, and the contributions, $\Delta I_{h|3}$ (red), caused by the distortion ΔV_3. for $h = 3$, 5, and 7.

Fig. 1 shows an example of the results for a sequence of tests in the presence of a harmonic voltage $\Delta V_3 = 2.3$ V [see Fig. 1(a)] applied to a CFL lamp. In Fig. 1(b), the loci of the harmonic domain components I_3, I_5, and I_7 are plotted together with the corresponding base currents, I_{bh}, and the contributions, $\Delta I_{h|3}$, caused by the distortion ΔV_3 for 24 different values of its phase angle.

III. New Test Procedure

In order to perform a comprehensive harmonic analysis with a single supply signal, the generation of a signal composed of a fundamental tone and a harmonic component, with linearly modulated phase, is proposed. The signal can be analytically expressed as

$$\bar{V}_T = A_1 \sin(\omega t) + A_h \sin(h \cdot \omega t + \varphi_h(t)) \tag{3}$$

and

$$\varphi_h(t) = \frac{2\pi}{T} \cdot t \tag{4}$$

where T is the period of the modulation. In this way, the initial phase angle of the harmonic components increases linearly with time and reaches the value of 2π after a period equal to T. Then, due to periodicity of the sine function, the phase angle returns to zero and starts to increase linearly again. This is shown in Fig. 2 which displays the phase angle modulated with a periodicity of 2 s: the modulating signal is essentially a sawtooth wave. Even if the phase angle has a different value for each time instant, the measurement of the phase difference between the fundamental and the harmonic components can be performed only when the fundamental component phase angle reaches zero. Therefore, for a 50-Hz system, measurement results can be taken each for 20 ms. This limits the phase resolution to

$$\Delta\varphi_h = 2\pi \frac{0.02}{T}. \tag{5}$$

The phase resolution can be improved by increasing T, but this will reflect on the memory requirement of generation system. A periodicity of 2 s is adopted in the following analysis in order to obtain the measurement of $N_\theta = 100$ different phase angles.

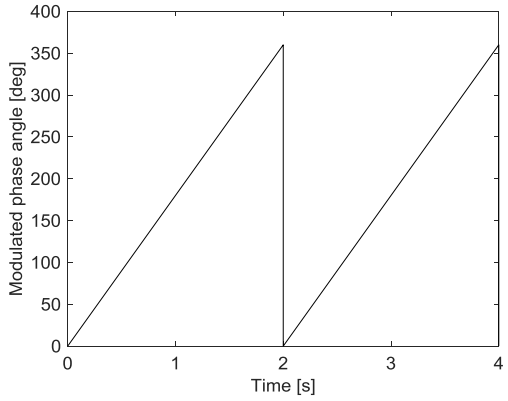

Fig. 2. Linear phase variation versus time.

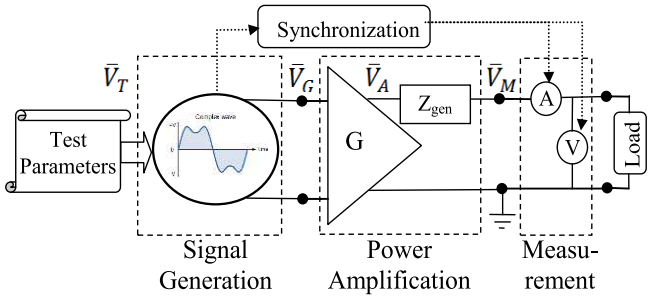

Fig. 3. Test bench simplified block diagram.

IV. Analysis and Characterization of Experimental Setup

A. Accuracy Analysis

In Fig. 3, a simplified block diagram of a hardware setup, which is able to test a specific electric load under steady-state (sinusoidal and nonsinusoidal) and dynamic (amplitude and phase modulation) conditions, is displayed. For the steady-state analysis considered in this paper, the amplitude, V_k^T, and phase, θ_k^T, for each harmonic component required to obtain the desired waveform, $\bar{V}_T$, should be defined. Adopting phasor notation, this can be represented as

$$\bar{V}_T = \sum_{k=1}^{K} V_k^T \cdot e^{j\theta_k^T} \cdot e^{jk\omega t} \tag{6}$$

where K is the highest harmonic order considered.

Typically, these test parameters are used to calculate the instantaneous values, equally spaced, within one period of a waveform with the same shape of desired test signal but with an amplitude scaled by a certain gain, G. These instantaneous values are sequentially and repetitively generated by a digital-to-analog (D/A) converter (signal generator) to obtain a real voltage signal, $\bar{V}_G$, that is successively amplified by a power amplifier, so obtaining $\bar{V}_A$.

In an ideal system

$$\bar{V}_G^{\text{ideal}} = \sum_{k=1}^{K} \frac{V_k^T}{G} \cdot e^{j\theta_k^T} \cdot e^{jk\omega t} \tag{7}$$

and

$$\bar{V}_A^{\text{ideal}} = G \cdot \bar{V}_G^{\text{ideal}} = \bar{V}_T. \tag{8}$$

However, each stage is able to introduce a systematic alteration, may be either linear or nonlinear, which will result in a deviation between the desired and the obtained signals. Linear effects simply introduce some modifications in the amplitude and phase angle of the harmonic components. Nonlinear effects are also able to introduce additional harmonic components. The real signal can be represented as

$$\bar{V}_G = \sum_{k=1}^{K} V_k^G \cdot e^{j\theta_k^G} \cdot e^{jk\omega t}. \tag{9}$$

Thus, a deviation from the desired waveform (an error) introduced due to the signal generation system is defined as

$$\bar{e}_G = \bar{V}_G - \frac{\bar{V}_T}{G} = \sum_{k=1}^{K} \left(V_k^G \cdot e^{j\theta_k^G} - \frac{V_k^T}{G} \cdot e^{j\theta_k^T} \right) \cdot e^{jk\omega t}. \tag{10}$$

Similarly, the output of amplifier can be represented as

$$\bar{V}_A = \sum_{k=1}^{K} V_k^A \cdot e^{j\theta_k^A} \cdot e^{jk\omega t}. \tag{11}$$

Accordingly, a deviation (an error) introduced by the amplification system is defined as

$$\bar{e}_A = \bar{V}_A - \bar{V}_T = \sum_{k=1}^{K} \left(V_k^A \cdot e^{j\theta_k^A} - V_k^T \cdot e^{j\theta_k^T} \right) \cdot e^{jk\omega t}. \tag{12}$$

In addition to systematic effects, each component of the generation stage is also able to introduce random fluctuations of waveform amplitude/parameters that could be considered and modeled as additional noise. Assuming an average value equal to zero, repeating the test conditions, and averaging help to reduce the effect of these errors on the results.

The overall deviation introduced by the generation chain results in a change of the considered test point, and this needs to be kept small so as to not affect the relevance of the test results. The amount of modifications, linear and nonlinear, systematic, and random, depends on the accuracy of the considered systems. However, the accuracy information commonly supplied by the manufacturers, or the calibration certificate, cannot be directly used to evaluate the specific contribution; so, a proper characterization procedure is often required for this aim.

One source of error which should be carefully considered is the power amplifier. As the amplification transfer function is not a pure gain G, it can introduce a different amplification and phase shift to each harmonic present in the signal, that is,

$$G \rightarrow \bar{G}(\omega) = G(\omega) e^{j\varphi_G(\omega)}. \tag{13}$$

To clearly describe this effect, let us consider a simple signal composed by only two components:

$$\bar{V}_T = V_1 \sin(\omega t) + V_h \sin(h \cdot \omega t + \theta_h) \tag{14}$$

where V_1 is the amplitude of the fundamental component and V_h and θ_h are the amplitude and phase of the hth harmonic component, respectively.

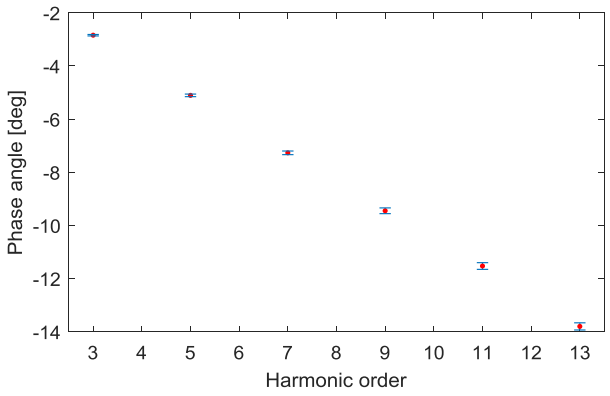

Fig. 4. Phase accuracy evaluated without phase angle correction: average value (red symbol) and standard deviation (blue whiskers).

After amplification, this becomes

$$\bar{V}_A = V_1 G(\omega)\sin(\omega t + \varphi_G(\omega)) + V_h G(h\omega)\sin(h\cdot\omega t + \theta_h + \varphi_G(h\omega)). \quad (15)$$

A flat response in amplitude for the accounted frequency should limit the relative amplitude changes. Negating the effect of the phase delay is more difficult to realize. In fact, for determining the harmonic phase angle, it is necessary to refer to the time instant when the fundamental component has zero phase. The effect of this additional phase for the fundamental component produces a time shift in the analysis equal to

$$\Delta t = \varphi_G(\omega)/\omega. \quad (16)$$

This time shift is present in the phase of each harmonic. This effect is proportional to the harmonic order and the harmonic phase angle at this time instant appears to be

$$\varphi_h(\Delta t) = h\cdot\varphi_G(\omega) + \varphi_h + \varphi_G(h\omega) \quad (17)$$

In this condition, the phase deviation in generation appears to be linearly increasing with harmonic order

$$e_h = \varphi_h - \varphi_h(\Delta t) = -h\cdot\varphi_G(\omega) - \varphi_G(h\omega). \quad (18)$$

An example of this effect, considered in [15] as system phase angle accuracy, is reported in Fig. 4. In the reported error bar, the center is the mean value and whiskers show the standard deviation of analyzed values. In this paper, all the graphs will be used with the same meaning. In the following paper, this effect is compensated before the assessment of experimental system performance.

A further linear modification is introduced by the supply current driven by the load under test, due to the output impedance of amplifier. This effect depends on the current magnitude. Knowledge about the actual voltage and current supplying the load (i.e., the actual test condition and load behavior) is obtained by the measurement system. Of course, measurement accuracy of adopted instrument is pre-eminent to obtain proper test results. Of course, accuracy of measurement instrument is vital for obtaining accurate test results. Similar to the generation system, common accuracy information about measurement instruments and signal transducers (if utilized) cannot be directly applied for assessing the expected accuracy

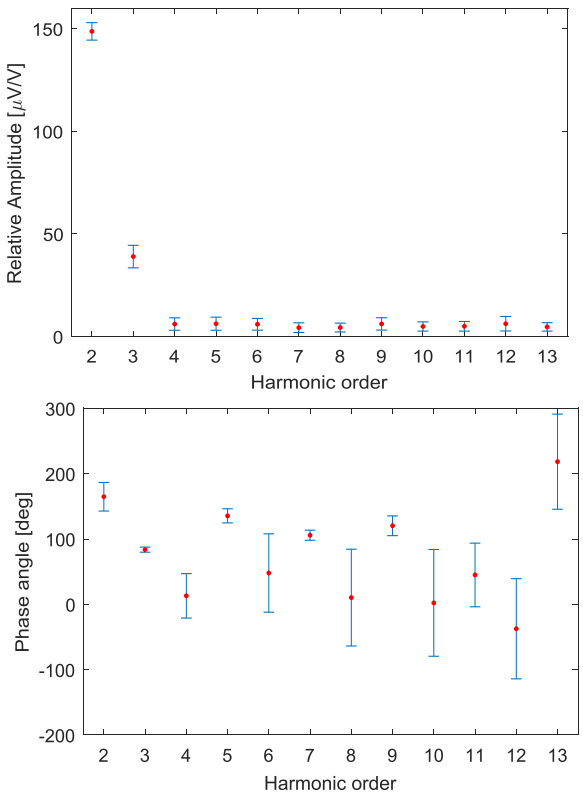

Fig. 5. Generated voltage, $\bar{V}_G$, accuracy for a pure sinusoidal waveform: average value (red symbol) and standard deviation (blue whiskers).

of measuring specific harmonics amplitude and phase angle, and a proper characterization process should be developed.

B. Metrological Characterization

For the implementation of the measurement system for the test bench shown in Fig. 3, a voltage data acquisition board (NI 9225, 300 V_{rms}, 24 bit, simultaneous sampling, 50 kHz, built-in antialias filters) and a current data acquisition board (NI 9227, 5 A_{rms}, 24 bit, simultaneous sampling, 50 kHz, built-in antialias filters) with high accuracy were utilized without any transducers. The sampling frequencies of the two boards (50 kHz) were synchronized. Both were referred to the same external master timebase clock obtained by exporting the clock used by the generation system (12.8 MHz). In this way, voltage and current sampling are synchronized with each other and the generation system, allowing for synchronized analysis.

The generation board used was the NI 5422 (16 bit, input range ± 12 V_{pk}, maximum sample rate 200 MHz, variable gain). The power amplifier was the ac power source AMX3120 ($P\text{max} = 12$ kVA, typical output total harmonic distortion (THD) lower than 0.10 %).

In order to characterize the metrological performance of the generation system, specific tests were designed. This is required as the spectral performance given by the manufacturer may not include all required frequencies (i.e., only at 50 kHz for low-voltage generator) and other parameters may not include sufficient detail (i.e., THD for power amplifier). This

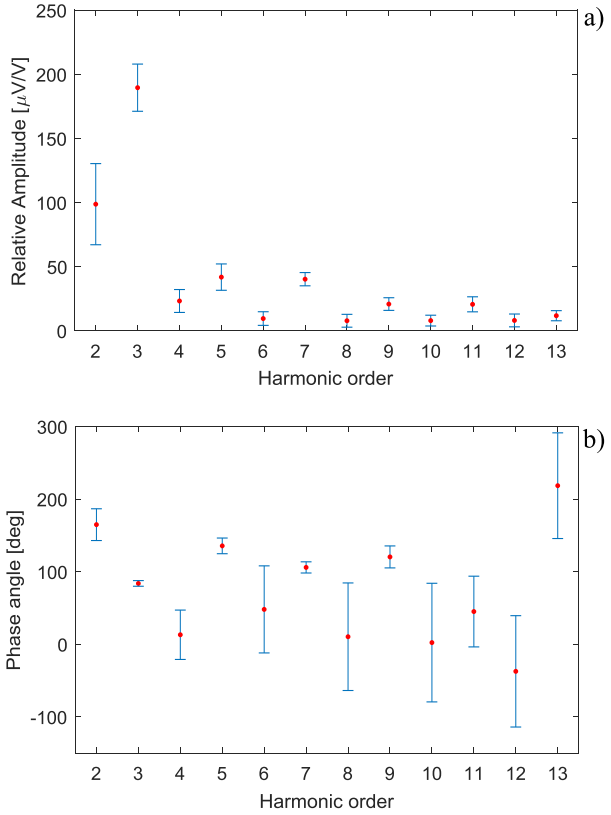

Fig. 6. Amplified voltage, $\bar{V}_A$, accuracy for a pure sinusoidal waveform: average value (red symbol) and standard deviation (blue whiskers).

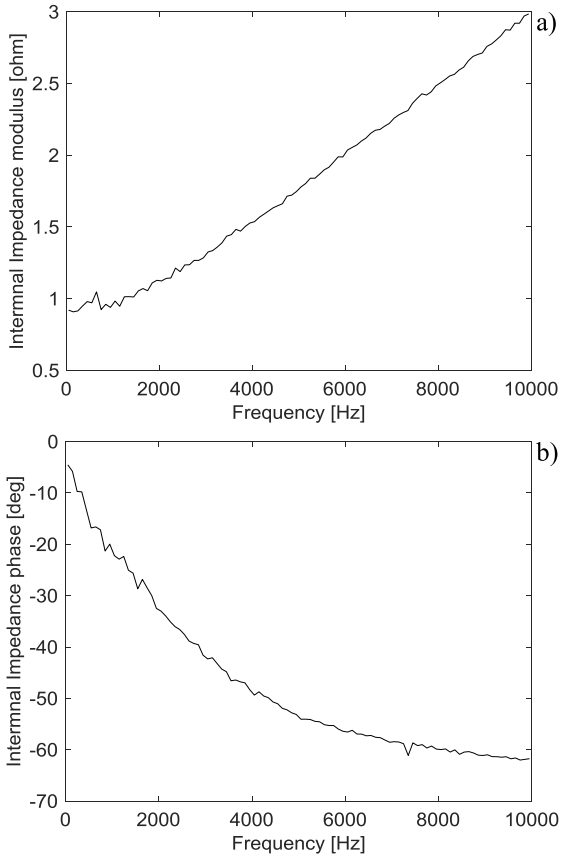

Fig. 7. Modulus and phase of internal amplifier impedance.

preliminary testing stage was performed with an open-circuit load due to the small amplitudes of currents involved in the considered tests, and the impact of the internal impedance of the power amplifier was estimated to be negligible.

For the first test, the waveform parameters were set to generate a pure sinusoidal component at 50 Hz, so, in theory, without harmonic components. The generated voltage ($\bar{V}_G$) and amplified signal ($\bar{V}_A$) were synchronously measured by the data acquisition system. The generation was repeated 1200 times and a synchronized spectral analysis was performed with the acquired samples to evaluate the harmonic contents both in terms of amplitude and phase angle. The harmonic phase angles were defined referring to the time instant of zero crossing of the fundamental component. Figs 5 and 6 show the harmonic components measured in the generated and amplified voltages, respectively.

It is worthwhile noting that for $\bar{V}_G$ (Fig. 5), the harmonic components over the third are mainly due to random effects (due to quantization in generation and other random noise sources) and so their phase angles have a limited relevance. Moreover, the nonlinear behavior of the amplifier introduces additional harmonics into $\bar{V}_A$. These components are the voltages applied to the equipment and represent a BG harmonic voltage that has to be taken into account in the test condition analysis. As stated in Section II-B, it is assumed that these are independent of the load.

Fig. 7 presents the value of output impedance measured with specific characterization experimental test. The test is performed in two stages. In the first stage, a signal composed by fundamental component at 50 Hz and only the kth harmonic component was generated and amplified without any load (open circuit). Both the generated and amplified signals are synchronously acquired. Then, the amplified signal was applied to a passive load (a resistor). During this stage, the current, $\bar{I}_G$, was acquired. Then, the kth harmonic component measured in voltage acquired without load was considered, $\bar{V}_k^A$ (without current, internal impedance produce no effect), the kth harmonic component measured in voltage acquired with load is, $\bar{V}_k^G$. So, the impedance at the kth harmonic frequency was calculated as

$$\bar{Z}_k^{\text{Gen}} = \left(\bar{V}_k^A - \bar{V}_k^G\right) \Big/ \bar{I}_k^G. \tag{19}$$

To properly account for the phase relation in (19), all the phase angles are referred to the phase of the generated signal. The generation and the acquisition tests were repeated for increasing harmonic orders up to 10 kHz. Fig. 8 reports the value of output amplification transfer function. In Fig. 8, the point at which the amplification decreases by 3 dB is also highlighted. So, the system has a frequency bandwidth that reaches 15 850 kHz. At this frequency, the corresponding phase delay is 98°. To achieve a higher precision, it is possible to refer to a different attenuation level (1 or 0.5 dB) decreasing the considered bandwidth. The global accuracies of the generation system, after correction of all the detected systematic deviations, are reported in Fig. 9 (for amplitude) and Fig. 10 (for phase angle).

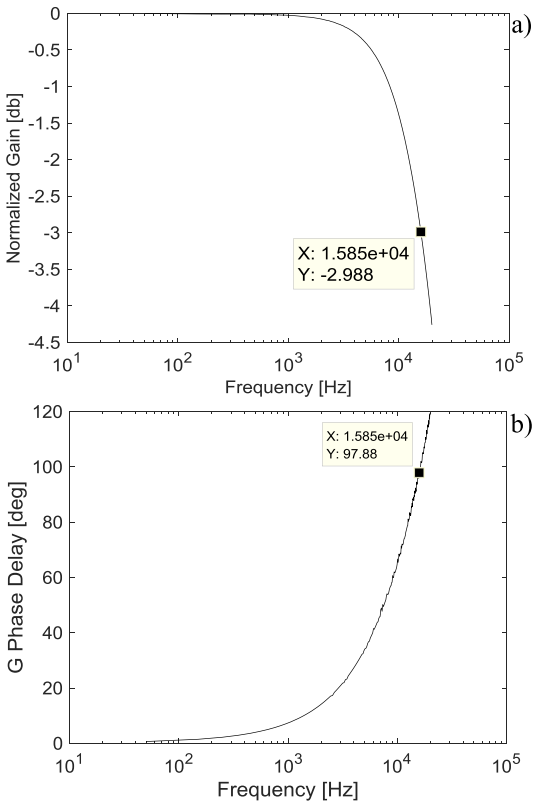

Fig. 8. Modulus and phase of amplifier transfer function with −3 dB point.

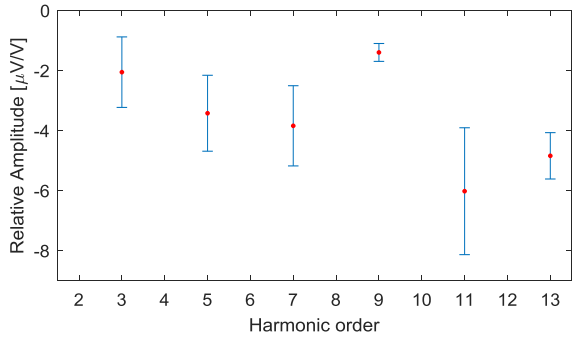

Fig. 9. Amplitude global accuracy of generation system after correction of all the detected systematic deviations: average value (red symbol) and standard deviation (blue whiskers).

V. Experimental Results

Measurements have been performed on a low-power, commercially available 20-W CFL lamp. Fifteen different levels of each BG harmonic voltage magnitude, ΔV_k, have been considered ranging from 0% to 140% of the EN50160 limits, V_{kLIM}, fixed, for each individual odd harmonic (from the 3rd to the 21st) [13].

The test corresponding to 0% amplitude was conducted to get the results for the base condition that was assumed to be the pure sinusoidal regime with 100% fundamental voltage.

Both the classical and the new test procedures have been implemented. Concerning the classical test procedure, the phase angle has been varied in the range from 0 to 2π in 24 equal spaced steps, $N_{\Delta\theta}$. For the new test procedure, the period of the phase modulated signal [see (4)] has been

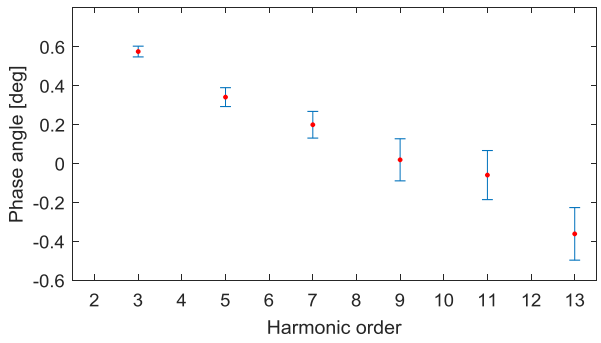

Fig. 10. Phase angle global accuracy of generation system after correction of all the detected systematic deviations: average value (red symbol) and standard deviation (blue whiskers).

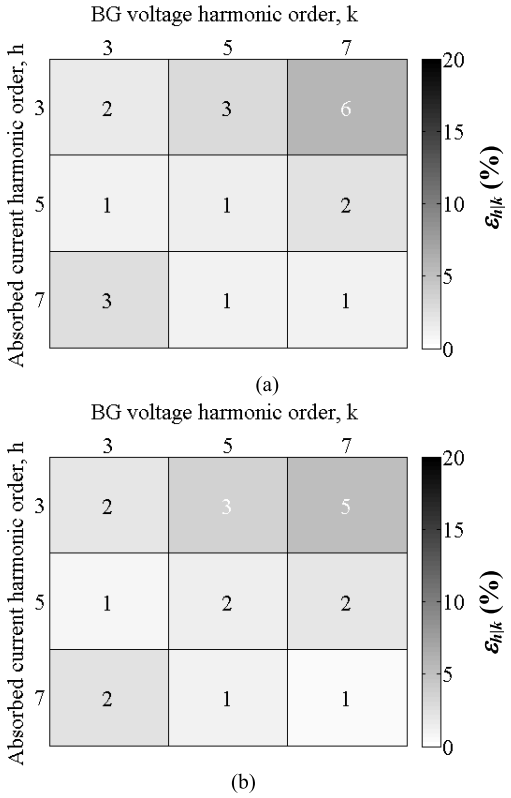

Fig. 11. Comparison of the norm of relative deviation, $\varepsilon_{h|}k$, between (a) classical test procedure and (b) new test procedure, for $\Delta V_k = 20\%$ of V_{kLIM} with $k = 3$, 5, and 7, and $h = 3$, 5, and 7.

chosen to be 2 s, which corresponds to $N_{\Delta\theta} = 100$ equivalent phase angle steps, having analyzed 200-ms length segments of the whole signal.

In synthesis, 3600 tests have been performed for the classical test procedure (15 voltage levels × 24 phase angles × 10 individual BG voltage harmonics) and 150 tests (15 BG voltage levels × 10 individual BG voltage harmonics) for the new proposed test procedure.

For the sake of brevity, only the results related to the effects of the first three odd harmonics of the BG voltage on the first three odd harmonics of the currents are reported.

The index used to quantify the performances of the two test procedures is the norm of the relative deviation calculated

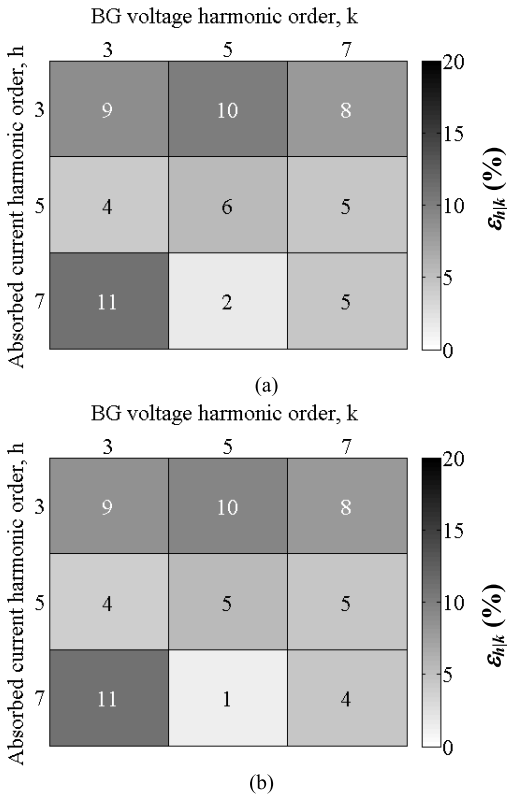

Fig. 12. Comparison of the norm of relative deviation, $\varepsilon_{h|k}$, between (a) the classical test procedure and (b) the new test procedure, for $\Delta V_k = 100\%$ of V_{kLIM} with $k = 3$, 5, and 7, and $h = 3$, 5, and 7.

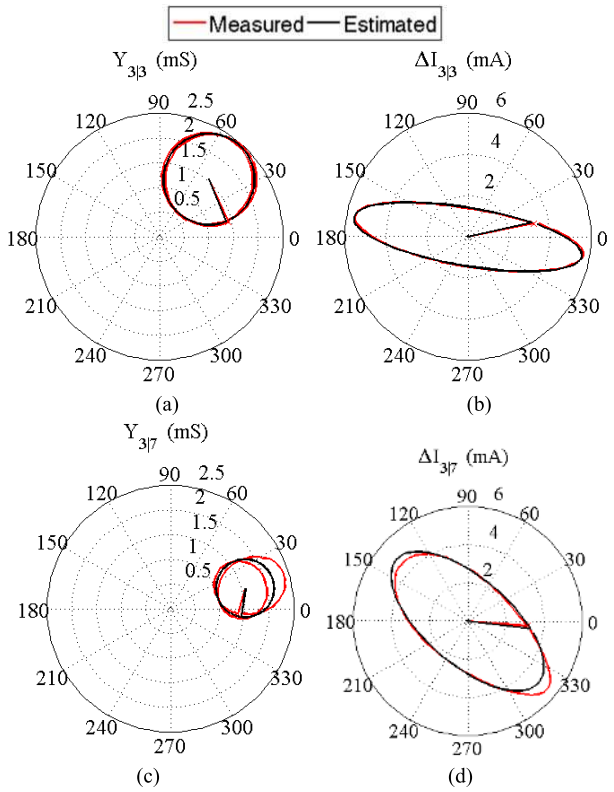

Fig. 13. Polar plot of (a) $Y_{3|3}$ and (b) $\Delta I_{3|3}$, for $\Delta V_3 = 20\%$ of $V_{3\mathrm{Lim}}$, and (c) $Y_{3|7}$, and (d) $\Delta I_{3|7}$, for $\Delta V_7 = 20\%$ of $V_{7\mathrm{Lim}}$. Red plots refer to measured data. Black solid lines refer to estimation by tensor parameterization.

using

$$\varepsilon_{h|k} = \sum_{j=1}^{N_{\Delta\theta}} \frac{\left\| \Delta I_{h|k}^{\mathrm{est}}(j) - \Delta I_{h|k}^{\mathrm{meas}}(j) \right\|}{\left\| \Delta I_{h|k}^{\mathrm{meas}}(j) \right\|} 100. \tag{20}$$

This index is intended to quantify the average accuracy of the estimated harmonic current variations, compared to the measured harmonic current variations, for a given value of the BG harmonic voltage magnitude and harmonic order.

Fig. 11 shows the comparison of the norm of the relative deviation $\varepsilon_{h|k}$ between the classical test procedure (a) and the new test procedure (b) for a BG harmonic voltage magnitude $\Delta V_k = 20\%$ of V_{kLIM}, with $k = 3$, 5, 7 and $h = 3$, 5, 7. Fig. 12 is similar to Fig. 11, but with $\Delta V_k = 100\%$ of V_{kLIM}.

It is possible to observe that the differences in the results of the two test procedures are extremely small, demonstrating that the accuracy of the new test procedure can be considered acceptable. Looking at Fig. 11(b), it is possible to observe that the deviations on the main diagonal are lower than 2%.

Fig. 13 shows the polar plots of (a) $Y_{3|3}$ and of (b) $\Delta I_{3|3}$ for BG harmonic magnitudes of 20% of the limits. Red plots refer to measured data; black solid lines refer to estimation by tensor parameterization; the two represented radii point to 0° phase angle of the applied BG voltage. It is possible to observe that the self-admittance, $Y_{3|3}$, draws a double circle on the complex plane, as expected from the theory for systems behaving linearly around the base point when a small magnitude of BG voltage is applied. This is also confirmed by the elliptic shape of the third harmonic current variation and by the almost perfect matching between measured and estimated quantities. On the other hand, looking at Fig. 13(c) and (d) where the $Y_{3|7}$ and $\Delta I_{3|7}$ are plotted, respectively, it is possible to observe that the effects of the seventh harmonic BG voltage on the third harmonic current show the evidence of a nonlinear transfer between the voltage and current: the locus of the measured admittance is no more a double circle while the estimated locus is still a double circle due to the linearity hypothesis. This is also confirmed by the relative deviation $\varepsilon_{3|7}$ in Fig. 11(b), i.e., 5%.

Fig. 14 is same as Fig. 13, but for BG harmonic magnitudes of 100% of the limits. It shows the polar plots of (a) $Y_{3|3}$ and (b) $\Delta I_{3|3}$, respectively, and similar considerations to those done for Fig. 13(c) apply, but in this case, the cause of the nonfulfillment of the linearity hypotheses is related to the higher BG voltage magnitude. The corresponding relative deviation, $\varepsilon_{3|3}$, in Fig. 12(b) is 9%. Finally, Fig. 14 shows the polar plots of (c) $Y_{7|3}$ and of (d) $\Delta I_{7|3}$, respectively, which correspond to the highest relative deviation, $\varepsilon_{7|3}$, in Fig. 12(b), i.e., 11%. In this case, the admittance locus shape is a closed-loop but very far from being a double circle, and the locus of the current deviations is no more an ellipse.

Finally, it is worth highlighting that the classical test procedures took 7.5 h, while the new procedure took only 1 h to be fully executed, resulting in a speed improvement of 7.5 times.

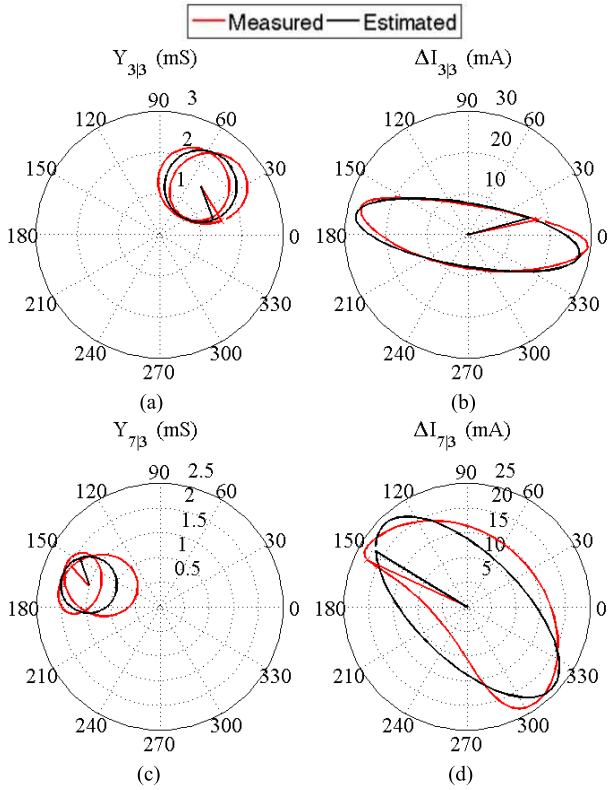

Fig. 14. Polar plot of (a) $Y_{3|3}$ and (b) $\Delta I_{3|3}$, for $\Delta V_3 = 100\%$ of $V_{3\text{Lim}}$, and (c) $Y_{7|3}$ and (d) $\Delta I_{7|3}$, for $\Delta V_3 = 100\%$ of $V_{3\text{Lim}}$. Red plots refer to measured data. Black solid lines refer to estimation by tensor parameterization.

VI. Conclusion

This paper has presented a new test procedure for the experimental evaluation of the frequency coupling matrix elements of power electronic devices. An automated test system has been designed, realized, and characterized from a metrological perspective. Experimental tests have shown the great speed improvement of the new test procedure in comparison to the classical test procedures presented in the literature with the same levels of accuracy of obtained results.

The main outcomes of this paper are as follows.

1) The procedure for the identification and the correction of the systematic errors of the test system was able to minimize the measurement uncertainty to at least one order of magnitude lower than the minimum deviation between model estimations and measurements.
2) The new test procedure for the identification of FTM based on phase-modulated nonsinusoidal signals, obtained the same accuracy as classical test procedures, while reducing the test duration of a factor 7.5.

The proposed test procedure offers particular benefits for applications requiring a larger number of experimental lab measurements, e.g., tests on families of equipment of different brands working in fixed operating conditions (e.g., lamps) or characterization of devices whose behavior is a function of operating power (electrical vehicles battery chargers or photovoltaic inverters).

Acknowledgment

This paper was prepared at the SUN-EMC Laboratory of the University of Campania "Luigi Vanvitelli."

References

[1] J. Arrillaga, B. C. Smith, N. R. Watson, and A. R. Wood, *Power System Harmonic Analysis*. New York, NY, USA: Wiley, 1997.
[2] A. Medina *et al.*, "Harmonic analysis in frequency and time domain," *IEEE Trans. Power Del.*, vol. 28, no. 3, pp. 1813–1821, Jul. 2013.
[3] E. V. Larsen, D. H. Baker, and J. C. McIver, "Low-order harmonic interactions on AC/DC systems," *IEEE Trans. Power Del.*, vol. 4, no. 1, pp. 493–501, Jan. 1989.
[4] B. C. Smith, N. R. Watson, A. R. Wood, and J. Arrillaga, "Harmonic tensor linearisation of HVDC converters," *IEEE Trans. Power Del.*, vol. 13, no. 4, pp. 1244–1250, Oct. 1998.
[5] Y. Sun, G. Zhang, W. Xu, and J. G. Mayordomo, "A harmonically coupled admittance matrix model for AC/DC converters," *IEEE Trans. Power Syst.*, vol. 22, no. 4, pp. 1574–1582, Nov. 2007.
[6] P. W. Lehn and K. L. Lian, "Frequency coupling matrix of a voltage-source converter derived from piecewise linear differential equations," *IEEE Trans. Power Del.*, vol. 22, no. 3, pp. 1603–1612, Jul. 2007.
[7] L. Frater, "Light flicker and harmonic modelling of electrical lighting," Ph.D. dissertation, Elect. Comput. Eng., Univ. Canterbury, Christchurch, New Zealand, 2015.
[8] M. F. Romero, L. E. Gallego, S. Müller, and J. Meyer, "Characterization of non-linear household loads for frequency domain modeling," *Ingeniería Invest.*, vol. 35, pp. 65–72, Dec. 2015.
[9] R. Senra, W. C. Boaventura, and E. M. A. M. Mendes, "Assessment of the harmonic currents generated by single-phase nonlinear loads," *Electr. Power Syst. Res.*, vol. 147, pp. 272–279, Jun. 2017.
[10] M. Fauri, "Harmonic modelling of non-linear load by means of crossed frequency admittance matrix," *IEEE Trans. Power Syst.*, vol. 12, no. 4, pp. 1632–1638, Nov. 1997.
[11] R. Langella, J. E. Caicedo, A. A. Romero, H. C. Zini, J. Meyer, and N. R. Watson, "On the use of fourier descriptors for the assessment of frequency coupling matrices of power electronic devices," presentation at the 18th Int. Conf. Harmon. Quality Power, Ljubljana, Slovenia, May 2018.
[12] J. E. Caicedo, A. A. Romero, H. C. Zini, R. Langella, J. Meyer, and N. R. Watson, "Impact of reference conditions on the frequency coupling matrix of a plug-in electric vehicle charger," presentation at the 18th Int. Conf. Harmon. Quality Power, Ljubljana, Slovenia, May 2018.
[13] M. Faifer, R. Ottoboni, M. Prioli, and S. Toscani, "Simplified modeling and identification of nonlinear systems under quasi-sinusoidal conditions," *IEEE Trans. Instrum. Meas.*, vol. 65, no. 6, pp. 1508–1515, Jun. 2016.
[14] M. Faifer, C. Laurano, R. Ottoboni, M. Prioli, S. Toscani, and M. Zanoni, "Definition of simplified frequency-domain volterra models with quasi-sinusoidal input," *IEEE Trans. Circuits Syst. I, Reg. Papers*, vol. 65, no. 5, pp. 1652–1663, May 2018.
[15] D. Gallo, C. Landi, R. Langella, M. Luiso, A. Testa, and N. Watson, "On the measurement of power electronic devices' frequency coupling admittance," in *Proc. Int. Workshop Appl. Meas. Power Syst. (AMPS)*, Liverpool, U.K., Sep. 2017, pp. 1–6.
[16] *Voltage Characteristics of Electricity Supplied by Public Distribution Networks*, Standard EN 50160, CENELEC, 2013.

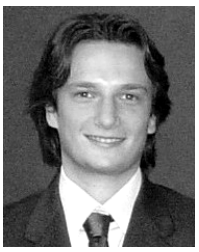

Daniele Gallo (S'00–M'04) was born in 1974. He received the Laurea degree in electronic engineering and the Ph.D. degree in electrical energy conversion from the University of Campania L. Vanvitelli, Aversa, Italy, in 1999 and 2003, respectively.

He is currently an Associate Professor with the University of Campania L. Vanvitelli. His current research interests include the setup of digital measurement instrumentation and the handling of automatic measurement systems.

Roberto Langella (S'00–M'01–SM'10) was born in Naples, Italy, in 1972. He received the Degree in electrical engineering from the University of Naples, Naples, Italy, in 1996, and the Ph.D. degree in electrical energy conversion from the University of Campania L. Vanvitelli, Aversa, Italy, in 2000.

He is currently an Associate Professor in electrical power systems with the University of Campania L. Vanvitelli.

Dr. Langella is a Senior Member of the IEEE Power Engineering Society.

Mario Luiso (S'07–M'08) was born in Naples, Italy, in 1981. He received the Laurea (*summa cum laude*) degree in electronic engineering and the Ph.D. degree in electrical energy conversion from the University of Campania L. Vanvitelli, Aversa, Italy, in 2005 and 2007, respectively.

He is currently an Assistant Professor with the Department of Engineering, University of Campania L. Vanvitelli. His current research interests include the development of innovative methods, sensors, and instrumentation for measurement of electrical, and, generally, physical quantities.

Dr. Luiso is a member of the IEEE Instrumentation and Measurement Society.

Alfredo Testa (M'83–SM'03–F'08) was born in Naples, Italy, in 1950. He received the Degree in electrical engineering from the University of Naples, Naples, Italy, in 1975.

He is currently a Professor in electrical power systems with the University of Campania L. Vanvitelli, Aversa, Italy. His current research interests include electrical power systems reliability and harmonic analysis.

Dr. Testa is a Fellow Member of the IEEE Power Engineering Society and the Italian Institute of Electrical Engineers.

Neville R. Watson (M'82–SM'99) received the B.E. (Hons.) and Ph.D. degrees in electrical engineering from the University of Canterbury, Christchurch, New Zealand.

He is currently a Professor with the University of Canterbury. His current research interests include power quality, harmonics, and electromagnetic transient analysis as well as computer modeling of electrical power systems.